

Article

Simulation of Isoprene Emission with Satellite Microwave Emissivity Difference Vegetation Index as Water Stress Factor in Southeastern China during 2008

Yuxiang Zhang ^{1,2} , Jiheng Hu ^{1,2} , Dasa Gu ³ , Haixu Bo ^{1,2}, Yuyun Fu ^{1,2} , Yipu Wang ^{1,2}  and Rui Li ^{1,2,*} 

¹ Comparative Planetary Excellence Innovation Center, School of Earth and Space Science, University of Science and Technology of China, Hefei 230026, China; zyx2012@mail.ustc.edu.cn (Y.Z.); hjh18305@mail.ustc.edu.cn (J.H.); bohx@mail.ustc.edu.cn (H.B.); fuyy11@mail.ustc.edu.cn (Y.F.); wypustc@mail.ustc.edu.cn (Y.W.)

² State Key Laboratory of Fire Science, University of Science and Technology of China, Hefei 230026, China

³ Division of Environment and Sustainability, Hong Kong University of Science and Technology, Hong Kong, China; dasagu@ust.hk

* Correspondence: rli7@ustc.edu.cn

Abstract: Isoprene is one of the most important biogenic volatile organic compounds (BVOCs) emitted by vegetation. The biogenic isoprene emissions are widely estimated by the Model of Emission of Gases and Aerosols from Nature (MEGAN) considering different environmental stresses. The response of isoprene emission to the water stress is usually parameterized using soil moisture in previous studies. In this study, we designed a new parameterization scheme of water stress in MEGAN as a function of a novel, satellite, passive microwave-based vegetation index, Emissivity Difference Vegetation Index (EDVI), which indicates the vegetation inner water content. The isoprene emission rates in southeastern China were simulated with different water stress indicators including soil moisture, EDVI, Normalized Difference Vegetation Index (NDVI) and Enhanced Vegetation Index (EVI). Then the simulated isoprene emission rates were compared to associated satellite top-down estimations. The results showed that in southeastern China, the spatiotemporal correlations between those simulations and top-down retrieval are all high with different biases. The simulated isoprene emission rates with EDVI-based water stress factor are most consistent with top-down estimation with higher temporal correlation, lower bias and lower RMSE, while soil moisture alters the emission rates little, and optical vegetation indices (NDVI and EVI) slightly increase the correlation with top-down. The temporal correlation coefficients are increased after applied with EDVI water stress factor in most areas; especially in the Yunnan-Guizhou Plateau and Yangtze River Delta (>0.12). Overall, higher consistency of simulation and top-down estimation is shown when EDVI is applied, which indicates the possibility of estimating the effect of vegetation water stress on biogenic isoprene emission using microwave observations.



Citation: Zhang, Y.; Hu, J.; Gu, D.; Bo, H.; Fu, Y.; Wang, Y.; Li, R. Simulation of Isoprene Emission with Satellite Microwave Emissivity Difference Vegetation Index as Water Stress Factor in Southeastern China during 2008. *Remote Sens.* **2022**, *14*, 1740. <https://doi.org/10.3390/rs14071740>

Academic Editor: Emanuele Santi

Received: 21 February 2022

Accepted: 1 April 2022

Published: 4 April 2022

Publisher's Note: MDPI stays neutral with regard to jurisdictional claims in published maps and institutional affiliations.



Copyright: © 2022 by the authors. Licensee MDPI, Basel, Switzerland. This article is an open access article distributed under the terms and conditions of the Creative Commons Attribution (CC BY) license (<https://creativecommons.org/licenses/by/4.0/>).

Keywords: passive microwave remote sensing; biogenic emission; vegetation water stress

1. Introduction

Isoprene (2-methyl-1, 3-butadiene, C_5H_8) is one of the most important volatile organic compounds (VOCs) in the atmosphere; playing an important role in the atmospheric chemistry related to ozone (O_3) and secondary organic aerosols (SOAs) [1–3], which are harmful to human bodies and crucial to the radiative forcing of surface. It is shown that increased isoprene emission can enhance ozone formation; resulting in about 50% change of ozone [4], and contribute to over half of the total SOAs production [5]. Generally, with the presence of nitrogen oxides (NOx), isoprene is initially oxidized by hydroxyl radical (OH, the principle oxidizing agent in atmosphere), nitrate radical (NO_3) and ozone etc.; thus influencing atmospheric total OH reactivity [6] and total ozone reactivity [7,8].

The intermediate products, such as methyl vinyl ketone (MVK), methacrolein (MACR), formaldehyde (HCHO) [6,9], can participate in other atmospheric chemical processes further [6]. Therefore, the studies of biogenic isoprene emission are necessary in regarding its regulation of the atmospheric chemistry and the alternation of future climate.

Terrestrial vegetation, especially forest, is the main source of isoprene [10,11]. Isoprene is found to be synthesized in tree leaves, and can increase the thermal tolerance of plants [12,13]; thus helping to survive in heat waves. The emission rate of isoprene depends on vegetation type and environmental conditions, such as temperature, radiation [14–19], CO₂ concentration and water supply [20–23], but how the emission responds to the daily environment is still under study throughout the world [24–27]. The annual global emission of isoprene by plants is estimated to be between 300 and 800 Tg C [14,28–30], which is much larger than the amount of anthropogenic emission [31]. Until now, isoprene emission rate at a large-scale is mainly estimated by top-down retrieval and bottom-up models.

The top-down retrieval method takes advantage of satellite observations and model simulations to estimate surface isoprene fluxes [32,33]. Assuming that there was a linear relationship between HCHO column density and land surface isoprene fluxes, Palmer et al. (2003, 2006) used the GEOS-Chem model to inverse satellite observed HCHO to surface isoprene emission in North America [34,35]. The method was then applied in other regions [36,37]. Currently, there are several satellite sensors which can measure the HCHO column density, such as the Global Ozone Monitoring Experiment (GOME), Ozone Monitoring Instrument (OMI) and Tropospheric Monitoring Instrument (TROPOMI). Among them, the OMI is commonly used in the reverse studies due to the long-term temporal coverage [38–41], and in this study, we also used the OMI top-down emissions for analysis.

These things considered, isoprene emission can be estimated by the bottom-up method. The bottom-up estimation is based on a physical or statistical model describing the relationship between the isoprene emission rate of vegetation and the controlling factors. In plants, isoprene is synthesized from multi-sources [42,43] through the 2-CMethyl-D-Erythritol 4-Phosphate (MEP) pathway in chloroplasts [43]. Numerous field studies showed that isoprene emission will increase with the raising of radiation and temperature. When the temperature is high, the emission will decrease after. In addition, other environmental factors, such as CO₂ concentration and water, can affect the emission [44]. Based on those results, bottom-up models are developed. The Model of Emission of Gases and Aerosols from Nature (MEGAN) is one of the most widely used bottom-up models, being coupled into chemical transport models such as WRF-Chem, Community Land Model (CLM) etc. [28,45]. MEGAN uses the emission factors (EFs) to quantify the potential VOCs emissions of different species, then applies the light-temperature algorithm and environmental stress algorithm to model the emission rates (ERs).

In the context of global warming induced spatial and temporal changes of the hydrological cycle, the effect of water stress on VOC emissions is raising attention, especially for tropics and subtropics. Water stress can largely affect the metabolism of vegetation by modifying the openness of stomata; directly affecting the leaf conductance to water and carbon exchanging process with the atmosphere [46,47]. The decrements of isoprene emission due to water stress are thought to be as high as 17–50% [48–50]. However, the response of isoprene emission to water stress is different from other vegetation activities. Studies showed that, when the drought starts with the decrease of soil moisture [44], the stomatal conductance and photosynthesis rate decline immediately, while isoprene emission remains constant at first because of the use of alternative cellular sources, then decreases after several days [51–53]. Therefore, although isoprene emission is affected by water stress, it is not directly sensitive to the change of soil moisture [42].

However, soil moisture is used as the stress factor of water supply in MEGAN v2.10 [28,30,45]. The algorithm introduces the wilting point of soil as the threshold of the response of isoprene emission to water stress. If soil moisture is lower than the wilting point, the plants cannot extract water from soil; thus the emission is completely stopped. Therefore, the soil moisture factor is highly sensitive to the soil moisture database because

the soil categories of different databases are varied [48,49]. In order to avoid such uncertainty, some modeling studies ignored the soil moisture factor (set the factor to 1) [29,54]. Some attempts were made by previous studies to improve the simulation using soil moisture. For example, multiple layers of soil were considered by Müller et al. (2008) [30]; Jiang et al. (2018) proposed a new factor using a photosynthesis parameter V_{cmax} and soil wetness factor β_t estimated by CLM [50]; and leaf temperature was added to revise the water stress factor by Out-Larbi et al. (2019) [55].

Although efforts were made to qualify the water stress effects on isoprene emission, studies were limited because of the use of soil moisture. In fact, the temporal variation of soil moisture cannot reflect the leaf water condition which affects biogenic emission. There are multiple parameters related to leaf water conditions that have been used to study the emission response to water stress. Plaza et al. (2005) found that in Mediterranean oak forest, the water xylem potential can serve as an indicator of drought [56]. Some experiments have found that the leaf water potential of oak shows a slower decrease than soil moisture over a long term [57], suggesting that the vegetation inner water content changes slower than soil moisture; thus the emission is not always correlated with soil water deficit [58]. Guidolotti et al. (2011) found the positive correlation between the isoprene emission rate of poplar and instantaneous water use efficiency [22]. Moreover, the leaf water potential, related to the leaf inner water content, showed a strong linear relationship with isoprene emission [53,58], which is recommended to represent the effects of water stress to the isoprene emissions in the model. Furthermore, the leaf water potential is positively correlated with the relative water content (the ratio of current vegetation water content to the saturated vegetation water content) [59]. Thus, the isoprene emission from vegetation is actually controlled by vegetation inner water content, instead of soil water content, and soil moisture is only a substitutional way to estimate the water stress effect.

However, very few, if any, satellite remote sensed vegetation water content index has been used for estimating isoprene emission. In recent years, a novel microwave-based vegetation index, Emissivity Difference Vegetation Index (EDVI), was found physically related to canopy water content in dense forest [60]. Until now, EDVI was utilized to represent the spatiotemporal variations of vegetation water content (VWC) and to estimate evapotranspiration [61]. Furthermore, EDVI was found to be positively correlated with the column density of HCHO; thus, biogenic emission [62]. Therefore, it is very promising that EDVI can be used as a stress factor to estimate the isoprene emission from vegetation.

In this paper, we developed a method to utilize EDVI as a water stress factor in the MEGAN model. In addition, soil moisture and two optical vegetation indices (OVIs), Normalized Difference Vegetation Index (NDVI) and Enhanced Vegetation Index (EVI), were also involved as reference. The results of all of the simulations in southeastern China during 2008 were compared with OMI top-down retrieval isoprene emission data.

2. Materials and Methods

2.1. Top-Down Retrieval Isoprene Emission

In order to get the long-term record of isoprene emission in a large area, top-down retrievals of isoprene emission based on OMI observed HCHO were used in this study. OMI is a sensor on board the Aura satellite launched in 2004, completing a global coverage almost in one day. The spatial resolution of OMI is $24\text{ km} \times 13\text{ km}$, which is suitable for the inversion. The top-down retrieval surface isoprene flux data are provided by the Tropospheric Modelling team of the Royal Belgian Institute for Space Aeronomy (BIRA-IASB), and are available on the website (<https://emissions.aeronomie.be/>), accessed on 31 December 2021). The inverse model is IMAGESv2 CTM; the driven meteorological fields are from the ERA-Interim reanalysis dataset from the European Centre for Medium-range Weather Forecasts (ECMWF); the anthropogenic emission data are from the Emission Database for Global Atmospheric Research (EDGAR4.2), the REASv2 inventory and RETRO inventory; pyrogenic data are from the Global Fire Emissions Database (GFED4s); and a priori biogenic data are from the MEGAN-MOHYCAN model [41,49]. To make the model

best fit the observed HCHO, the iterative quasi-Newton optimization algorithm is coupled with the model and used to calculate the biogenic isoprene emissions fit the observation best [49]. Although the top-down retrieval emissions have not been fully evaluated, in this paper, we believed the top-down retrieved isoprene fluxes, especially the variation of the fluxes, are closer to the actual biogenic isoprene emission rates because of the constraint of satellite observed HCHO. In southeastern China, HCHO is always available, which ensures the isoprene emission is fully constrained [49].

2.2. MEGAN Models

The Model of Emission of Gases and Aerosols from Nature (MEGAN) was first released in 2006 [28], and updated to version 2.10 in 2012 [45]. It can be run coupled with chemical transport models, or run independently when providing the meteorological inputs, land cover type data (LC), emission factors (EFs), and vegetation leaf area index (LAI). The isoprene emission rate (ER) is given by:

$$ER = \gamma \cdot EF = \gamma \cdot \sum_i EF_i \cdot \chi_i, \quad (1)$$

EF_i is the emission factor of vegetation type i , and χ_i is the fraction of that vegetation type in the given grid. γ is the emission activity factor reflecting the response of biogenic emission to the variations of environmental conditions (light, temperature, leaf age and soil moisture).

$$\gamma = C_{CE} \cdot \gamma_P \cdot \gamma_{T_ld} \cdot \gamma_{LAI} \cdot \gamma_{age} \cdot \gamma_{sm}, \quad (2)$$

C_{CE} , the canopy environment coefficient, was set to a value (0.57) that results in $\gamma = 1$ for the standard conditions based on Guenther et al. (2012). γ_{T_ld} is the light-dependent temperature factor, γ_P is the light factor, γ_{LAI} is the LAI factor, γ_{age} is the factor considering leaf age, and γ_{sm} is the factor accounting for soil moisture. The detailed algorithms of the factors, γ_{T_ld} , γ_P , γ_{age} and γ_{LAI} , are described by Guenther et al. (2006, 2012) [28,45].

The last term, soil moisture factor γ_{sm} , is calculated by:

$$\gamma_{sm} = \begin{cases} 1 & \text{when } SM > \theta_1 \\ \frac{SM - \theta_w}{\theta_1 - \theta_w} & \text{when } SM > \theta_w \text{ and } SM < \theta_1, \\ 0 & \text{when } SM < \theta_w \end{cases} \quad (3)$$

The parameter θ_w (m^3/m^3) is the soil wilting point, and the θ_1 (m^3/m^3) is the soil saturating point. θ_1 was set as $0.06 + \theta_w$ in 2006 [28] and was changed to $0.04 + \theta_w$ in 2012 [45]. In this study, we used the latest one, $0.04 + \theta_w$. Based on the algorithm, the soil wilting point θ_w can affect the factor greatly and should be different values according to the soil moisture databases. For example, Müller et al. (2008) used a value of 0.171 when using ECMWF soil moisture data [30]. In the study, the Weather Research and Forecasting (WRF) v3.9.1 model simulation was used to provide the soil moisture, so the wilting points should be taken correspondingly [63]. The default soil type in WRF v3.9.1 is shown in Figure 1a and the corresponding wilting points in WRF v3.9.1 are listed in Table 1.

We used the WRF v3.9.1 model driven by the National Center for Environmental Prediction FiNaL (NCEP FNL) data to provide the hourly input meteorological fields. The simulated area was from latitude 0 to 60 N, and longitude 70 E to 140 E with a spatial resolution of 0.25 degree over the year 2008, and a small part (southeastern China, latitude from 15 to 40, longitude from 100 to 125) was selected out after the simulation. The WRF simulation used the Morrison 2-moment microphysics scheme, Grell–Freitas cumulus parameterization scheme, RRTMG longwave and shortwave radiation physics scheme, YSU boundary layer scheme, and Noah land surface scheme [64]. Then the 2-m temperature (T2), downwelling shortwave flux (SWDNB), 10-m wind speed (U10 and V10), rain (RAINNC and RAINC), pressure (P), 2-m vapor mixing ratio (Q2), soil temperature (TSLB), and moisture (SMOIS) of the first layer of soil (5 cm in WRF) were extracted from the WRF

simulation outputs. These hourly data were then used to drive MEGAN to estimate the daily emission.

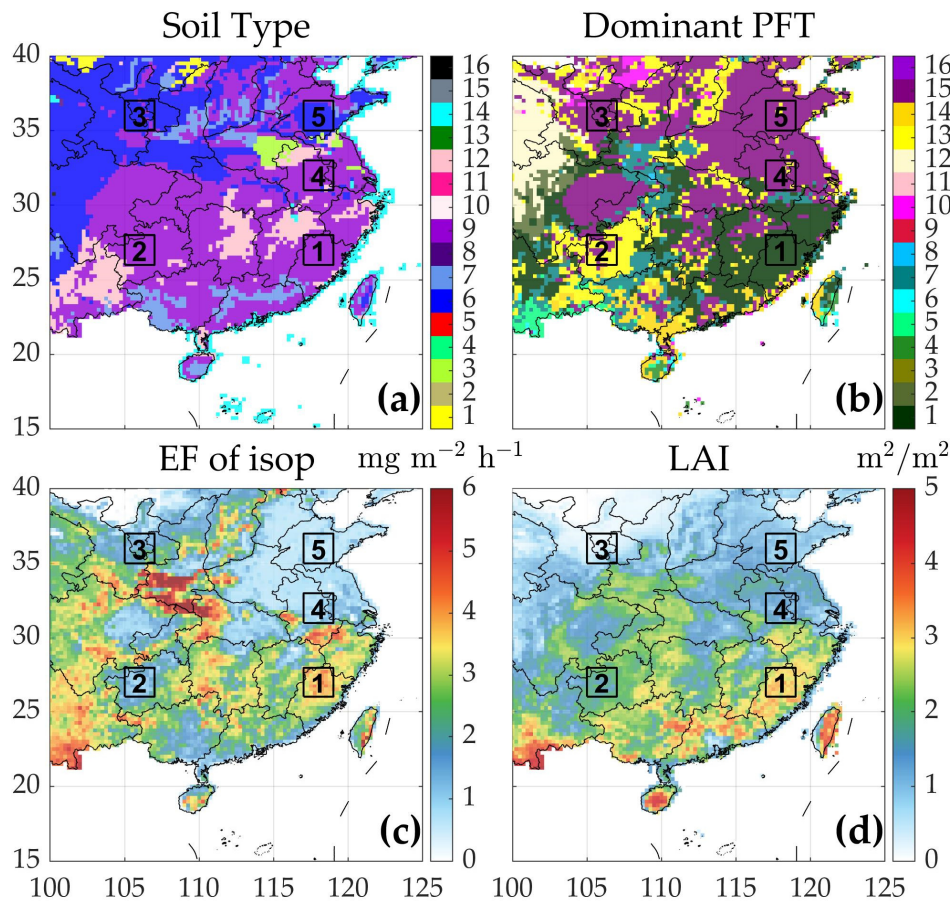


Figure 1. The spatial distribution of: (a) the soil types; (b) the dominant plant functional type (PFT); (c) the emission factor (EF) of isoprene ($\text{mg m}^{-2} \text{ h}^{-1}$); (d) the annual mean LAI. The soil types are listed in Table 1 and the PFTs are listed in Table 2.

Table 1. The classification of soil types and the corresponding wilting points in WRF.

Class	Name	Wilting Point θ_w (m^3/m^3)
1	Sand	0.01
2	Loamy Sand	0.028
3	Sandy Loam	0.047
4	Silt Loam	0.084
5	Silt	0.061
6	Loam	0.066
7	Sandy Clay Loam	0.069
8	Silt Clay Loam	0.120
9	Clay Loam	0.103
10	Sandy Clay	0.100
11	Silty Clay	0.126
12	Clay	0.138
13	Organic Matter	0.066
14	Water	-
15	Bedrock	0.006
16	Other	0.028

The data of EFs (0.0083 degree resolution) and Plant Functional Types (PFTs) (0.05 degree resolution) are available at <https://bai.ess.uci.edu/megan/data-and-code/megan21> (accessed on 31 December 2021). LAI data (0.05 degree resolution) are derived from the Global Land Surface Satellite Leaf Area Index (GLASS LAI 8-day) product (<http://glass-product.bnu.edu.cn/>, accessed on 31 December 2021). All the data were collected and regridded to 0.25 degree to match the WRF simulations. The spatial distribution of PFTs, soil type, EFs and averaged LAI are presented in Figure 1; the description of soil types and PFTs are listed in Tables 1 and 2. In southeastern China, the dominant soil types (Figure 1a) are loam, clay and clay loam. In the south, there is mainly clay loam, while in the north, there is mainly loam. Trees are mainly located in the south, such as Fujian, Zhejiang and Jiangxi (Figure 1b). In the North China Plain (NCP) and Sichuan Basin (SB), the dominant PFT is crop. The EF map of isoprene (Figure 1c) shows consistent spatial patterns with PFTs because trees are greater emitters than crops or grass. In the areas covered by trees, such as Yunnan, Guangdong, Fujian and the north of Sichuan Basin, the EFs are much higher, around $4 \text{ mg m}^{-2} \text{ h}^{-1}$, reaching $6 \text{ mg m}^{-2} \text{ h}^{-1}$ in the north of Sichuan. While in those areas mainly covered by sparse vegetation (grass or crop), the EFs are relatively lower, about $1\text{--}2 \text{ mg m}^{-2} \text{ h}^{-1}$. In addition, the averaged LAI in the NCP and SB where crops are dominant is lower, and in the forest, LAI is higher than $3 \text{ m}^2/\text{m}^2$ (Figure 1d), which demonstrates the higher biomass in the forest.

Figure 2a presents the annual mean soil moisture simulated by WRF. Soil moisture is high in the south, such as Fujian, Yunnan and Guizhou. And in the cropland, such as SB and NCP, soil moisture is relatively lower.

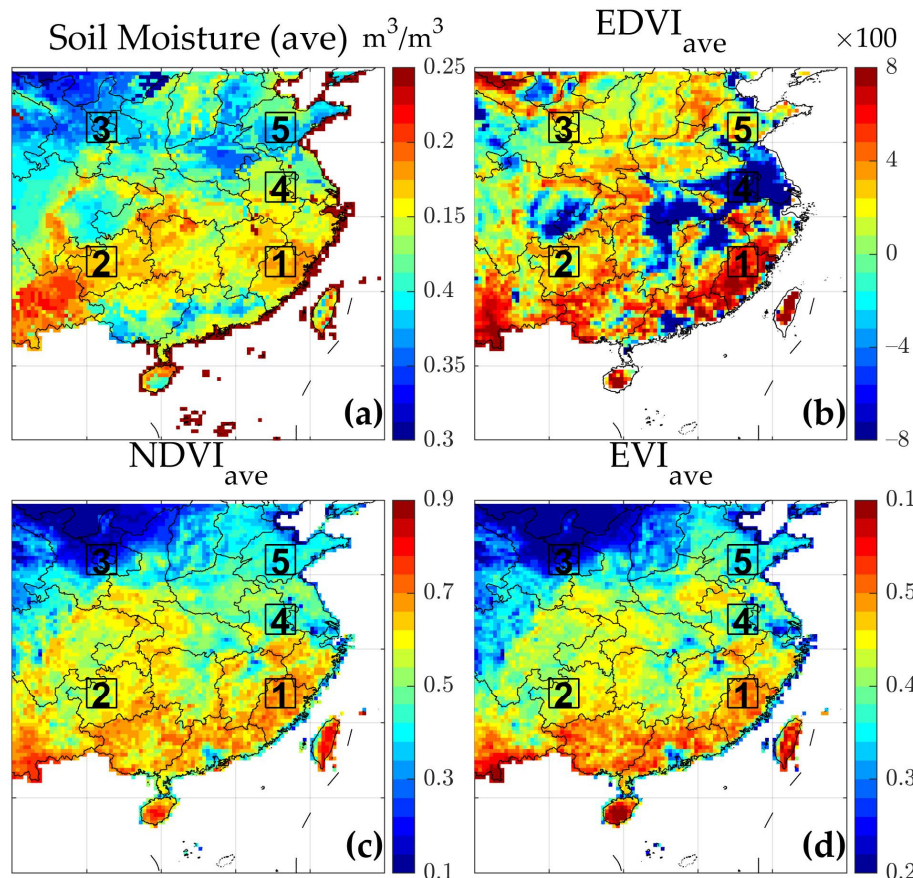


Figure 2. The spatial distribution of annual mean: (a) soil moisture simulated by WRF; (b) EDVI; (c) NDVI; (d) EVI.

Table 2. The classification of plant functional types.

Class	Plant Functional Type
1	Needleleaf Evergreen Temperate Tree
2	Needleleaf Deciduous Boreal Tree
3	Needleleaf Evergreen Boreal Tree
4	Broadleaf Evergreen Tropical Tree
5	Broadleaf Evergreen Temperate Tree
6	Broadleaf Deciduous Tropical Tree
7	Broadleaf Deciduous Temperate Tree
8	Broadleaf Deciduous Boreal Tree
9	Broadleaf Evergreen Temperate Shrub
10	Broadleaf Deciduous Temperate Shrub
11	Broadleaf Deciduous Boreal Shrub
12	Arctic C3 Grass
13	Cool C3 Grass
14	Warm C3 Grass
15	Crop
16	Corn

2.3. EDVI, EDVI Factor and Optical VI Factors

EDVI is defined as the difference of microwave land surface emissivity (MLSE) between 18.7 GHz and 36.5 GHz [60]:

$$\text{EDVI}_p = \frac{\text{MLSE}_p^{36.5} - \text{MLSE}_p^{18.7}}{0.5 (\text{MLSE}_p^{36.5} + \text{MLSE}_p^{18.7})}, \quad (4)$$

The MLSE data are retrieved from the Advanced Microwave Scanning Radiometer for EOS (AMSR-E), with ~20 km spatial resolution and daily temporal resolution [65], which is much higher than optical VIs (16 day for MODIS NDVI, for example). 'p' is the polarization of the MLSE, and here, vertical polarized EDVI was used for study because the vertical component was higher correlated with moisture content of vegetation [66]. Please refer to Li et al. (2020) for the details of EDVI retrieval in China [67].

In southeastern China, EDVI is a good indicator of the vegetation water content, and is positively correlated with NDVI, but their seasonal variation phases are different [67]. A characteristic of microwave-based EDVI differing from optical VIs is that it can be obtained from satellite in both clear sky and in non-raining cloudy sky; thus EDVI can be retrieved daily. In this paper, we compared the effects of EDVI and two optical VIs (NDVI and EVI from MOD13C1) to the MEGAN simulated isoprene emission. The optical VIs (NDVI and EVI) were interpolated to daily temporal resolution linearly to suit the simulation.

The annual mean of EDVI, NDVI and EVI in 2008 in southeastern China are shown in Figure 2b–d. Around the Yangtze River, EDVI is relatively lower because of the low value of open water and wet soil. This is consistent with Li et al. (2020) [67]. NDVI and EVI show lower values only around the lakes. In other places, the patterns of EDVI, NDVI and EVI are similar. In the south, such as Fujian, Guangxi and Yunnan, EDVI is high, about 0.008; NDVI is about 0.8; and EVI is larger than 0.4, showing higher VWC and greenness there. While in the North China Plain (NCP), EDVI is about 0.004; NDVI is about 0.4; and EVI is around 0.3, which indicates lower VWC and greenness in the cropland. In the northwest, NDVI and EVI are quite low, but EDVI is high, this is because EDVI is highly affected by the snow in winter [67]. According to the spatial distributions of PFTs (Figure 1a), soil type (Figure 1b) and the latitudes, five typical regions (Table 3) were selected, as shown in Figures 1 and 2. The time series of soil moisture, EDVI, NDVI and EVI in the regions are presented in Figure 3.

Table 3. The center locations, dominant PFT, soil types and emission factor (EF) in the selected five regions. The numbers of PFTs and soil types refer to the classes listed in Tables 1 and 2 and the values in the bracket are the percentage of the class in the region.

Region	Latitude	Longitude	PFT	Soil	EF ($\text{mg m}^{-2} \text{h}^{-1}$)
1	27	118	1 (58.3%) 7 (27.4%)	9 (100%)	3.7
2	27	106	13 (42.4%) 15 (36.2%)	9 (100%)	1.4
3	36	106	15 (46.0%) 13 (10.3%)	6 (87.5%) 9 (12.5%)	1.7
4	32	118	15 (47.9%) 13 (23.8%)	9 (92.2%) 8 (3.1%)	1.0
5	36	118	15 (47.9%) 13 (22.2%)	6 (82.8%) 9 (14.1%)	0.8

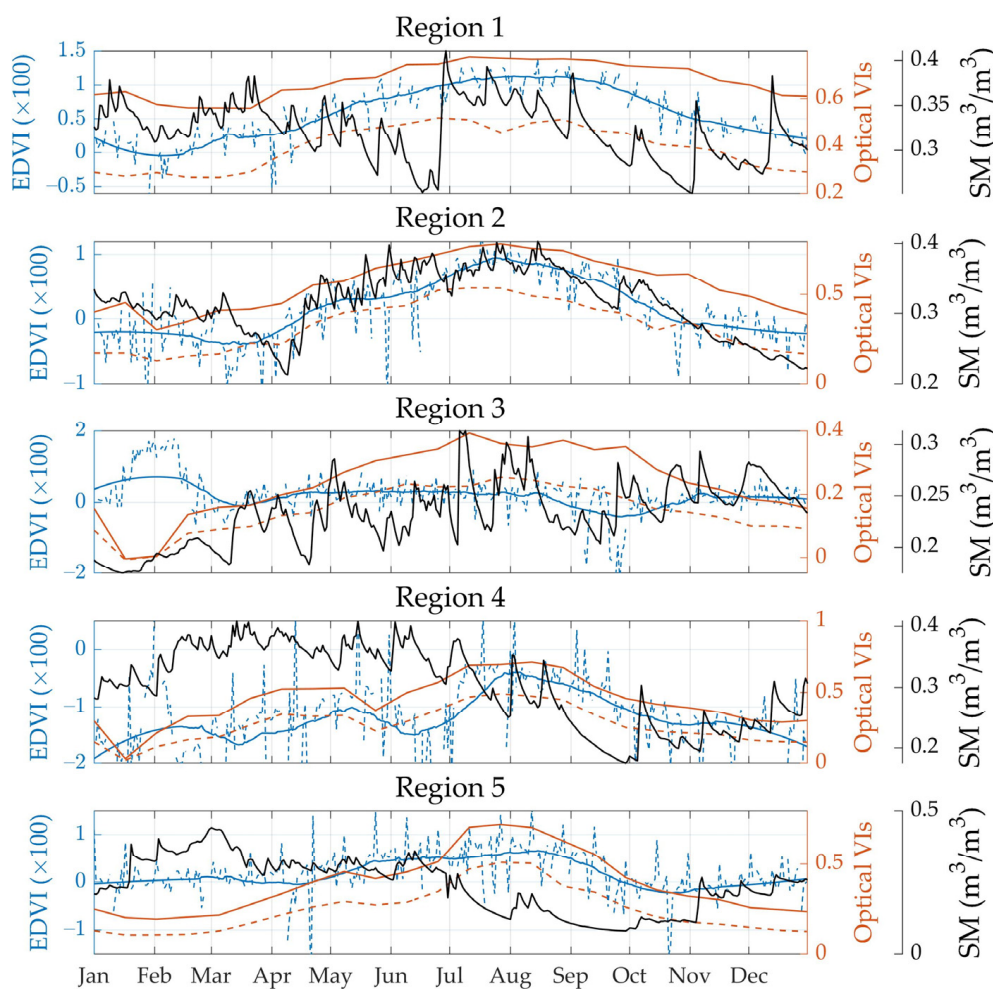


Figure 3. The time series of soil moisture (SM, black line), EDVI (blue line), NDVI (red line) and EVI (red dash line) in the selected five regions. The blue dash line denotes the daily EDVI, and the blue line denotes the 30-day smoothed EDVI.

As shown in Figure 3a, in region 1, mainly covered by forest, the soil moisture is higher than $0.25 \text{ m}^3/\text{m}^3$ all year round, and EDVI is higher than 0. The mean soil moisture there is about $0.32 \text{ m}^3/\text{m}^3$; being stable in spring, but fluctuating in other seasons. In February, EDVI starts to increase, and reaches the highest value, about 0.01, around August. NDVI

and EVI show similar temporal patterns, but the two start to increase in March [67]. The annual mean NDVI is 0.68 and EVI is 0.4, showing the dense vegetation in the region.

The dominant PFT in region 2 is grass with significant seasonality. Soil moisture is highest in late spring and summer, and decreases in autumn. EDVI, NDVI and EVI show similar seasonal variations with soil moisture, which increase around March and start to decrease around August. The mean EDVI is about 0.001, lower than that in region 1 (mean EDVI is 0.006). The mean NDVI and EVI are low too, about 0.57 and 0.33, demonstrating the sparse vegetation.

Region 3 is located in the northwest, dominated by cropland (Figure 1b). Soil moisture is lower than $0.2 \text{ m}^3 / \text{m}^3$ in January and February, and starts to increase after. NDVI and EVI are higher around July, indicating the growth of crops. In late January and early February, EDVI increases quickly to over 0.01, while NDVI and EVI decline to about 0. By combining the snow data (MYD10C1), it is believed that the vegetation indices are heavily influenced by winter snow (see Appendix A for details).

The dominant PFTs in region 4 and region 5 are both crops, with relatively lower EDVI, NDVI and EVI. In the two regions, the values of NDVI and EVI are similar (0.45 and 0.27 in region 4; 0.40 and 0.25 in region 5), showing that the vegetation densities in the two regions are close. All of the three vegetation indices show strong seasonal variations. NDVI and EVI start to increase in March, and reach the first peak around early May, and then increase to another peak around August. The first peak of EDVI is around mid-May, later than NDVI or EVI. EDVI in region 4 is about -0.012 , while in region 5 is 0.002, indicating the larger fraction of open water and bare soil in region 4.

From Figure 3, it is shown that in the northwest (region 3), vegetation indices are affected by the winter snow heavily (Figure A1 in Appendix A), leading to the increase of EDVI and decrease of optical VIs. In other places, the indices are well consistent to present vegetation conditions. Although the value of EDVI varies in different places (regions 4 and 5), EDVI can capture the temporal variations of VWC [67].

Studies showed that isoprene emission is linearly correlated with leaf water potential [58]. So, to study the effects of the change of VWC to the biogenic emission, we employed EDVI to present the VWC, i.e., large EDVI means no water stress, and low EDVI means high water stress. Furthermore, based on the framework of MEGAN, stress factor should be a value between 0 and 1 [45]. Thus, the EDVI-based water stress factor is described as a function of EDVI in the following formula:

$$\gamma_{\text{EDVI}} = \frac{\text{EDVI} - \text{EDVI}_{\min}}{\text{EDVI}_{\max} - \text{EDVI}_{\min}}, \quad (5)$$

where EDVI_{\min} and EDVI_{\max} denote the minimum and maximum of EDVI through the year, respectively. So, the value of γ_{EDVI} is between 0 and 1, and is linearly changed with increasing EDVI.

For the purpose of evaluation and comparison, we also designed the other three water stress factors using smoothed EDVI, NDVI and EVI:

$$\gamma_{\text{SEDVI}} = \frac{\text{SEDVI} - \text{EDVI}_{\min}}{\text{EDVI}_{\max} - \text{EDVI}_{\min}}, \quad (6)$$

$$\gamma_{\text{NDVI}} = \frac{\text{NDVI} - \text{NDVI}_{\min}}{\text{NDVI}_{\max} - \text{NDVI}_{\min}}, \quad (7)$$

$$\gamma_{\text{EVI}} = \frac{\text{EVI} - \text{EVI}_{\min}}{\text{EVI}_{\max} - \text{EVI}_{\min}} \quad (8)$$

SEDVI means smoothed EDVI (such as blue dash lines in Figure 3). To retain the seasonal variation of EDVI, but exclude the daily variation, we smoothed EDVI in 30 days. γ_{SEDVI} here is used to present the effect of the daily variation of EDVI to the simulated emission. NDVI and EVI were first interpolated linearly to daily, and then applied to the calculation of γ_{NDVI} and γ_{EVI} .

2.4. MEGAN Simulations

To compare and evaluate the impacts of soil moisture, and those vegetation indices on isoprene emission, we conducted six simulations in 2008 using MEGAN. S0 is the base simulation without any water stress. S1 is the simulation with the soil moisture factor ($S1 = S0 * \gamma_{SM}$). S2 is the simulation with the EDVI stress factor ($S2 = S0 * \gamma_{EDVI}$) as the water stress factor. S3 is the simulation with the smoothed EDVI factor ($S3 = S0 * \gamma_{SEDVI}$). S4 is the simulation with the NDVI factor ($S4 = S0 * \gamma_{NDVI}$). S5 is the simulation with the EVI factor ($S5 = S0 * \gamma_{EVI}$). All six simulations were compared with OMI top-down retrieval isoprene emission data.

3. Results

The averaged isoprene emissions in 2008 from satellite top-down retrieval and the six simulations are shown in Figure 4. It can be seen that the top-down annual mean isoprene emission rate is relatively low with maximum emission less than $0.6 \text{ mg m}^{-2} \text{ h}^{-1}$ (Figure 4a). The emission is higher in the south of Shaanxi, the north of Jiangxi and Hainan, about $0.4 \text{ mg m}^{-2} \text{ h}^{-1}$, and is quite low in the areas covered by short vegetation, such as the North China Plain (NCP), lower than $0.1 \text{ mg m}^{-2} \text{ h}^{-1}$. From a spatial view, all of the six simulations show a generally consistent spatial pattern with high spatial correlation coefficients ($R > 0.8$), with different bias due to different water stress factors. Among them, S0 (without water stress) and S1 (soil moisture as water stress factor) show the largest area mean bias of $0.09 \text{ mg m}^{-2} \text{ h}^{-1}$ (relative bias = 65%) because of no water stress applied. S2 and S3 (EDVI and smoothed EDVI as water stress factors) show the smallest mean bias of $0.02 \text{ mg m}^{-2} \text{ h}^{-1}$, i.e., the relative bias decreases from 65% to 12% after applying EDVI factor, which means the EDVI water stress factors alters the emission rates close to top-down. S4 and S5 (optical vegetation indices as water stress factors) show medium bias of $0.05 \text{ mg m}^{-2} \text{ h}^{-1}$ and $0.03 \text{ mg m}^{-2} \text{ h}^{-1}$. The root mean squared errors (RMSEs) of top-down and simulations show the same patterns. The RMSEs of S0 and S1 are largest ($0.11 \text{ mg m}^{-2} \text{ h}^{-1}$), and the RMSEs of S2 and S3 show the lowest (about $0.07 \text{ mg m}^{-2} \text{ h}^{-1}$), while the RMSEs of S4 and S5 are moderate (about $0.09 \text{ mg m}^{-2} \text{ h}^{-1}$), indicating the uncertainty is decreased when EDVI factor is applied. Generally, from Figure 4, it is presented that the simulated isoprene emissions are all spatially consistent with top-down emission with different levels of overestimation, and the simulations with EDVI water stress factors show the lowest bias and RMSE.

To investigate the effects of the different water stress factors on isoprene emission, the time series of those factors in the five regions selected are shown in Figure 5. The relationships between simulated daily emissions and top-down emission are presented in Figure 6, and the monthly averaged results are presented in Figure 7.

It is obvious that, due to the linear algorithm, the temporal variations of the vegetation factors (Figure 5) are quite similar with the variations of the indices (Figure 3). First of all, in regions 1, 2, 3 and 4, soil moisture is always high, leading to the constant SM factor (constant 1) throughout the whole year; while in region 5, the soil moisture decreases in September and is lower than the wilting point, leading to the decrease of SM factor. It is noticed that, in region 5, the decrease of soil moisture in September is small, but leads to the large decrease of SM factor. The abrupt decline may induce high uncertainty during the period [49]. The other factors (EDVI, NDVI and EVI) follow the seasonality of vegetation growth; thus show similar temporal variations in each region. Generally, the factors are higher in the summer and lower in the winter. The values of EDVI factors and SEDVI factors in the five regions are all larger than 0.4; NDVI factors and EVI factors vary from 0 to 1. In region 1, the EDVI factor and SEDVI factor are lowest in early February, and increase until August, while the NDVI factor and EVI factor start to increase in March. In region 2, the NDVI factor and EVI factor start to increase during February, while the EDVI factor and SEDVI factor start to increase in March. In region 3, due to the influence of the snow in winter, the EDVI factor and SEDVI factor show a peak in early February, while the NDVI factor and EVI factor show a valley in late January. In region 4, NDVI and EVI

factors show two peaks through the year, one in April and another in July, while the EDVI factor shows one in May and another in July, and another in January because of the snow. In region 5, the EDVI factor and SEDVI factor are relatively stable, while the NDVI factor and EVI factor are higher in July and August. In September, the SM factor decreases, but other factors don't show a significant decrease, indicating that, although the soil moisture is decreasing, vegetation doesn't lose water as fast.

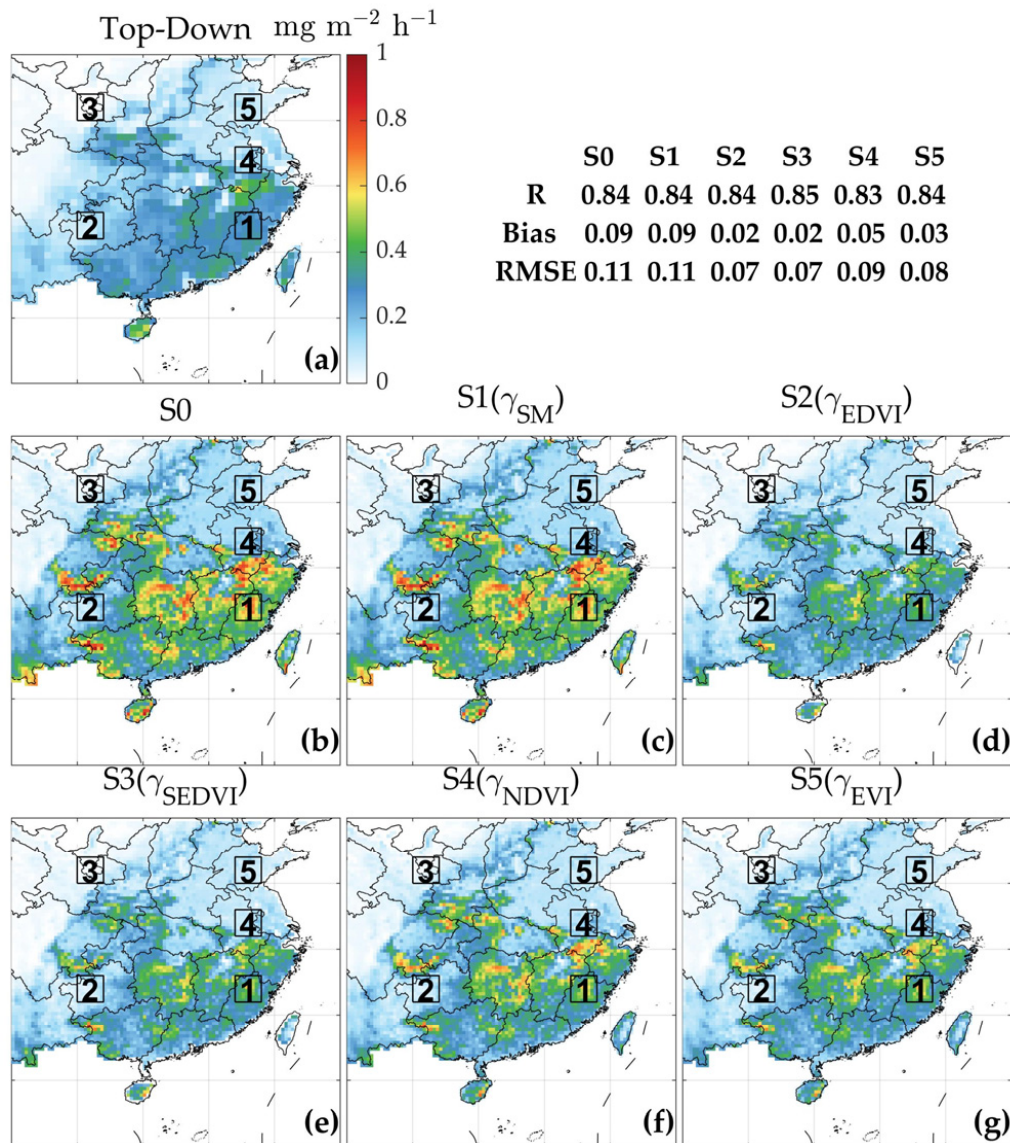


Figure 4. The spatial distribution of the averaged isoprene emission of (a) top-down; (b) S0 (without water stress); (c) S1 (with soil moisture factor); (d) S2 (with EDVI factor); (e) S3 (with SEDVI factor); (f) S4 (with NDVI factor); (g) S5 (with EVI factor). The table on the upper-right shows the spatial correlation coefficients (R), mean bias ($\text{mg m}^{-2} \text{h}^{-1}$) and root mean squared error (RMSE, $\text{mg m}^{-2} \text{h}^{-1}$) between the six simulations (S0 to S5) and top-down.

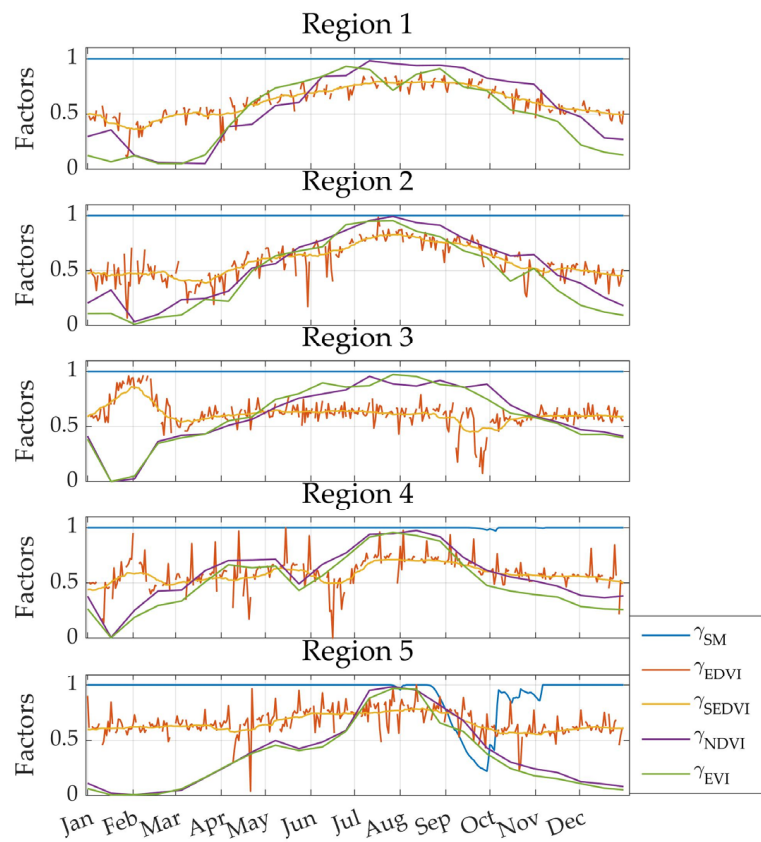


Figure 5. The time series of daily water stress factors during 2008 (blue: SM factor, red: EDVI factor, yellow: SEDVI factor, purple: NDVI factor, green: EVI factor.).

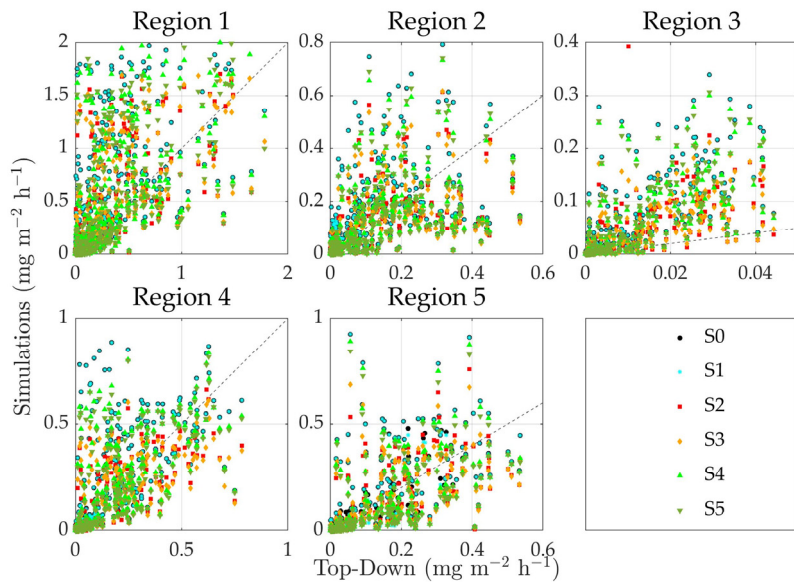


Figure 6. The scatter plots of the daily top-down emission versus the daily simulated emissions in the five regions, the dash line denotes 1:1 line. (black circle: S0 versus top-down, green square: S1 versus top-down, red square: S2 versus top-down, orange diamond: S3 versus top-down, light green upward-pointing triangle: S4 versus top-down, green downward-pointing triangle: S5 versus top-down).

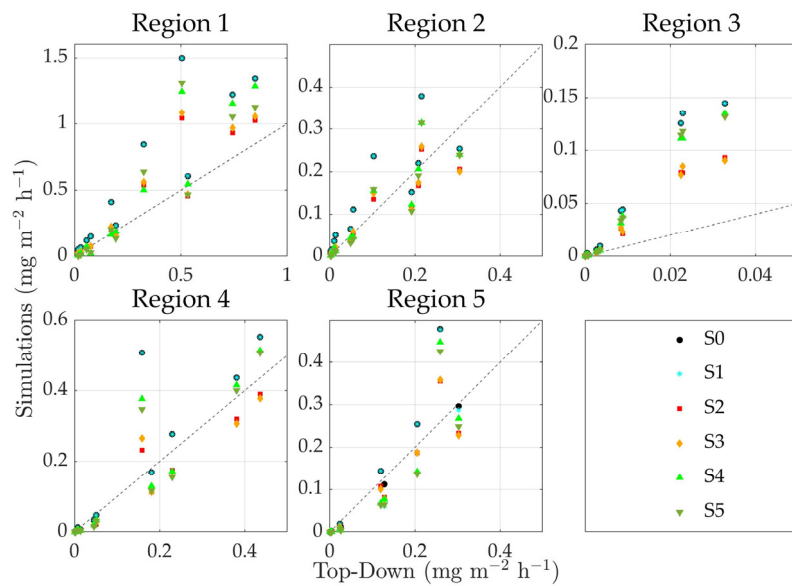


Figure 7. The scatter plots of the monthly top-down emission versus the monthly simulated emissions in the five regions, the dash line denotes 1:1 line. (black circle: S0 versus top-down, green square: S1 versus top-down, red square: S2 versus top-down, orange diamond: S3 versus top-down, light green upward-pointing triangle: S4 versus top-down, green downward-pointing triangle: S5 versus top-down).

We compared the simulated daily emissions and top-down emission (Figure 6); the statistics are presented in Table 4, and the monthly results are shown in Figure 7 and Table 5. Generally, in all of the five regions, the simulated emissions are also consistent with the top-down emission, with higher values in some regions, which may be resulted from the overestimated emission factors. Especially in region 3, the top-down emission is nearly zero, suggesting the low emission intensity, while the simulated emission is about $0.1 \text{ mg m}^{-2} \text{ h}^{-1}$, about 10 times higher than the top-down emission.

Table 4. The daily statistics between the six simulations and top-down emissions. The statistics include CORR (daily temporal correlation coefficient), bias ($\text{mg m}^{-2} \text{ h}^{-1}$), and RMSE (root mean squared error, $\text{mg m}^{-2} \text{ h}^{-1}$).

Region	Statistics	S0	S1	S2	S3	S4	S5
1	CORR	0.62	0.62	0.66	0.65	0.66	0.64
	Bias	0.255	0.255	0.085	0.101	0.142	0.126
	RMSE	0.477	0.477	0.350	0.363	0.420	0.415
2	CORR	0.55	0.55	0.63	0.59	0.60	0.59
	Bias	0.031	0.031	-0.013	-0.010	0.000	-0.004
	RMSE	0.133	0.133	0.101	0.106	0.115	0.116
3	CORR	0.67	0.67	0.61	0.67	0.66	0.67
	Bias	0.034	0.034	0.017	0.018	0.028	0.029
	RMSE	0.061	0.061	0.039	0.035	0.054	0.054
4	CORR	0.71	0.71	0.81	0.74	0.74	0.74
	Bias	0.045	0.045	-0.019	-0.018	0.013	0.006
	RMSE	0.162	0.162	0.101	0.114	0.138	0.134
5	CORR	0.72	0.70	0.74	0.72	0.69	0.69
	Bias	0.021	0.015	-0.008	-0.008	-0.005	-0.010
	RMSE	0.122	0.124	0.094	0.097	0.113	0.108

Table 5. The monthly statistics between the six simulations and top-down emissions. The statistics include CORR (monthly temporal correlation coefficient), bias ($\text{mg m}^{-2} \text{h}^{-1}$), and RMSE (root mean squared error, $\text{mg m}^{-2} \text{h}^{-1}$).

Region	Statistics	S0	S1	S2	S3	S4	S5
1	CORR	0.91	0.91	0.93	0.93	0.94	0.90
	Bias	0.255	0.255	0.087	0.101	0.141	0.126
	RMSE	0.306	0.306	0.171	0.184	0.254	0.260
2	CORR	0.86	0.86	0.93	0.91	0.91	0.90
	Bias	0.031	0.031	-0.012	-0.010	0.001	-0.004
	RMSE	0.062	0.062	0.041	0.045	0.045	0.048
3	CORR	0.99	0.99	0.99	0.98	0.99	0.99
	Bias	0.034	0.034	0.017	0.018	0.028	0.029
	RMSE	0.047	0.047	0.025	0.025	0.041	0.041
4	CORR	0.90	0.90	0.97	0.95	0.93	0.93
	Bias	0.045	0.045	-0.019	-0.018	0.014	0.006
	RMSE	0.103	0.013	0.038	0.049	0.074	0.068
5	CORR	0.94	0.92	0.94	0.94	0.89	0.89
	Bias	0.021	0.015	-0.007	-0.008	-0.005	-0.010
	RMSE	0.065	0.070	0.039	0.041	0.065	0.062

In terms of the difference among vegetation types, forest (region 1, Figure 6) shows the largest isoprene emission rate by top-down and simulation among the five regions, which confirms that the capacity of releasing VOCs from trees is much stronger than crop, grass and other short vegetation. The maximum emission rate in forest is about $2 \text{ mg m}^{-2} \text{ h}^{-1}$, significantly higher than that in other regions. The simulated emission rates are all highly temporally correlated with top-down emission, with correlation coefficients of 0.65. The correlation coefficients of S2 (using EDVI factor) and S4 (using NDVI factor) are a little higher (0.66). In addition, S2 and S3 show the minimum bias ($0.085 \text{ and } 0.101 \text{ mg m}^{-2} \text{ h}^{-1}$) with top-down, which means EDVI decreased the relative bias from 86% to about 30%. The RMSEs of S2 and S3 also decrease to 0.350 and $0.363 \text{ mg m}^{-2} \text{ h}^{-1}$, indicating a higher consistency with top-down emission.

In the southeastern grassland (region 2), the emissions are moderate, with the largest emission rates over $0.5 \text{ mg m}^{-2} \text{ h}^{-1}$. The temporal correlations of S2 to S5 and top-down are all higher than S0, while that of S1 is the same as S0 due to the constant value of the SM factor. The increases of temporal correlations of S2 to S5 indicate that the emission is affected by vegetation conditions. The correlation of S2 and top-down is the highest among all of the simulations, reaching 0.63, which is 0.08 larger than S0, with small bias ($-0.013 \text{ mg m}^{-2} \text{ h}^{-1}$) and the lowest RMSE ($0.101 \text{ mg m}^{-2} \text{ h}^{-1}$). The corresponding relative bias decreased from 32% to -13%, which suggests the more coincident results with top-down.

In regions 3, 4 and 5, EDVI is affected by winter snow in January and February (Figures 3, 5 and A1), so we compared the results including and excluding the first 2 months (January and February), but the results show the same because the emission rates in the 2 months are nearly zero; thus the influence of water stress is negligible. Therefore, we will not distinguish the snow season, even though snow will affect vegetation indices.

In region 3, located in the northwest, the emission is low. The top-down estimated maximum emission rate is less than $0.05 \text{ mg m}^{-2} \text{ h}^{-1}$, while the model simulations show less than $0.4 \text{ mg m}^{-2} \text{ h}^{-1}$, indicating the large uncertainties here. The correlations of S0, S1, S3, S5 and top-down are highest among the simulations, reaching 0.67, while the simulation applying daily EDVI factor (S2) shows a lower correlation coefficient, about 0.61. For bias and RMSE, it is shown that S2 and S3 with EDVI are closer to the top-down estimation. Generally, in northwestern China, the vegetation is sparse, the isoprene emission is low, and the estimation is highly uncertain.

In region 4, mainly covered by crop, the maximum of the emission rate is about $1 \text{ mg m}^{-2} \text{ h}^{-1}$ estimated both by simulation and top-down. The correlation coefficient of S0 and top-down is high, about 0.71, showing the simulation is highly temporally consistent with top-down. After applying EDVI factor (S2), the correlation coefficient is significantly increased to 0.81, while other simulations (S3 to S5) show only moderate increase (0.74 and 0.76). In addition, the bias of S2 ($-0.019 \text{ mg m}^{-2} \text{ h}^{-1}$) drops to less than half of S0 ($0.045 \text{ mg m}^{-2} \text{ h}^{-1}$), and the RMSE ($0.101 \text{ mg m}^{-2} \text{ h}^{-1}$) is lowest among all of the simulations, indicating the highest consistency of S2 and top-down in this region.

Different from other regions, in region 5, soil moisture factor is not constant. However, S1 shows even lower correlation than S0, indicating the soil moisture factor cannot present the real change of vegetation water condition; thus leading to the decrease of temporal correlation. The other two factors (NDVI and EVI factors) show similar results. The correlation coefficients of S4 or S5 are all decreased, suggesting the inaccurate estimation of vegetation water stress using optical VIs, i.e., NDVI and EVI. Compared with other simulations, by using EDVI factor, S2 shows the highest correlation among those simulations, reaching 0.74, and both the bias and RMSE are decreased. The corresponding relative bias decreases from 23% to -9% , and RMSE is also reduced to 76%, showing the better estimation of water stress by EDVI factor.

From the monthly results (Figure 7 and Table 5), the temporal coefficients of simulations and top-down are much higher than daily results with values over 0.9. Generally, among all of the simulations, S2 shows the highest temporal correlation coefficients and lowest RMSE in most regions, especially in regions 2 and 4 where the correlation coefficients increased about 0.07 compared with S0, and RMSE decreased 34% and 63% separately. The relative biases of S2 are relatively low too, especially in region 1, decreasing from 87% to 30%. Overall, the monthly results are similar with the daily results with higher temporal correlations.

The temporal correlation coefficients of the simulations and top-down estimations are then calculated in each grid. The spatial distributions of the daily correlation coefficients are shown in Figure 8 and the monthly results are shown in Figure 9. To present the differences among the six simulations, we also conducted the differences in pairs: S1-S0, effect of SM factor; S2-S0, effect of EDVI factor; S3-S0, effect of SEDVI factor; S4-S0, effect of NDVI factor; S5-S0, effect of EVI factor; S2-S3, effect of daily EDVI factor than smoothed EDVI factor (SEDVI factor).

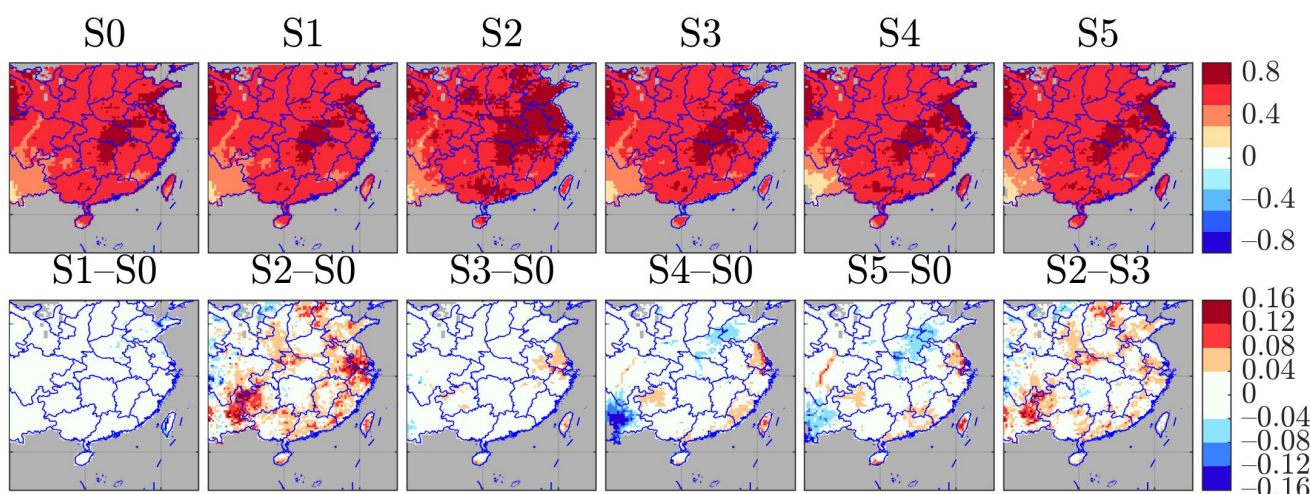


Figure 8. The spatial distributions of the daily temporal correlations between top-down and the six simulations (first row), and the differences of the correlations (second row).

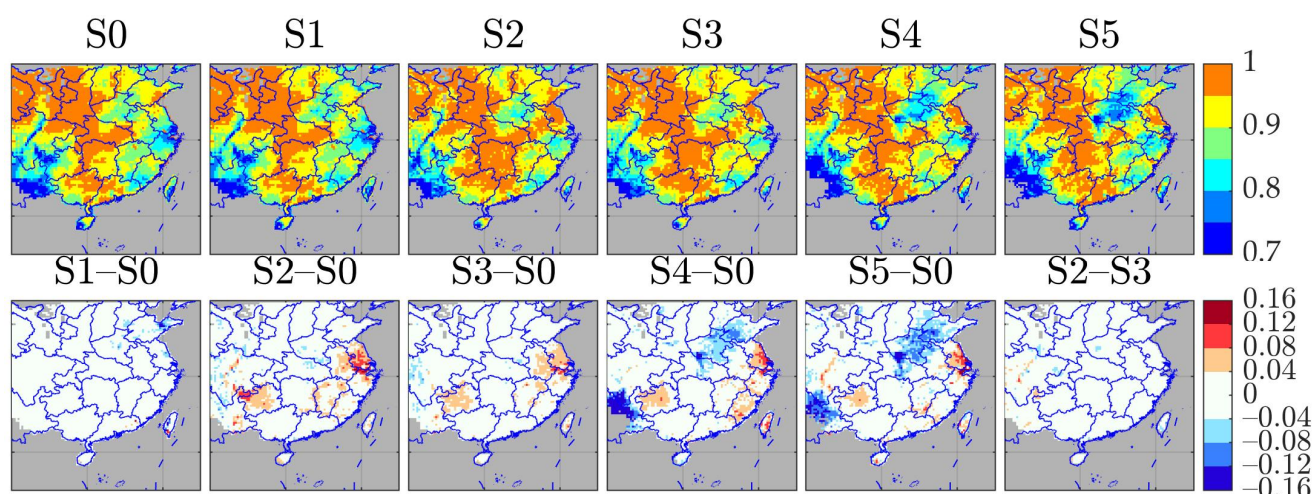


Figure 9. The spatial distributions of the monthly temporal correlations between top-down and the six simulations (first row), and the differences of the correlations (second row).

It is shown that all of the simulations can capture the main temporal variations of emission presented by top-down retrieval (first row in Figure 8); the correlation coefficients are larger than 0.6 in most places. In the south of Yunnan, R is relatively low, about 0.2. In the Yangtze Basin (especially around Hubei), R is high, reaching 0.8. Comparing S1 to S5 with S0, it is found that S2 shows the largest improvement on the correlation (S2-S0), such as in Yunnan, Yangtze River Delta, Fujian etc. There is almost no improvement of S1 in southeastern China, due to the constant SM factor. In NCP, S1 even shows lower correlation than S0, indicating that soil moisture fails to present water stress there. Compared with S3, the correlation coefficients of S2 are much larger (>0.16) than S0 in the Yangtze River Delta (YRD) and Yunnan-Guizhou Plateau, indicating the simulation using EDVI, especially daily EDVI, is more consistent with top-down. S4 and S5 show different patterns in different places. In Yunnan and NCP, the correlation coefficients of S4 and S5 are lower than S0, and in YRD are larger, about 0.08. The moderate improvement of NDVI and EVI suggest that optical vegetation indices are quite limited in presenting vegetation water content.

Monthly results (Figure 9) show the similar patterns. The correlations are all high, over 0.8 in most areas (first row in Figure 9). The differences (second row in Figure 9) also demonstrate that the simulation using daily EDVI as water stress factor shows the most consistent temporal variation with top-down emission in the Yangtze River Delta (YRD) and Yunnan-Guizhou Plateau.

Generally, it can be seen that compared with soil moisture and other vegetation indices, using EDVI, especially daily EDVI, to indicate the water stress for plants can better improve the temporal correlation of MEGAN simulated isoprene emission with top-down retrievals in southeastern China.

In conclusion, we applied EDVI, NDVI and EVI to MEGAN to simulate isoprene emission rates, and compared these with satellite top-down retrieved emissions in southeastern China. Because top-down isoprene fluxes are constrained using monthly OMI HCHO observations [49], we presented both the daily and monthly regional averaged results, as shown in Figures 6 and 7 and Tables 4 and 5. The daily results and monthly results are consistent and robust, and reveal that the simulated emission using EDVI is closer to the top-down retrieval in the southeast, especially in the places covered by dense vegetation. It is shown that the use of the EDVI factor will result in a better estimation of water stress on biogenic emission.

4. Discussion

Most research is still limited to the soil moisture, but numerous field studies have shown that the emission is weakly sensitive to soil moisture or photosynthesis [22,53,58]. It

is shown that short-term drought will not inhibit, but stimulate the biogenic VOCs emission because of the low water stress and higher temperature during the drought. However, long-term drought will decrease the emission because of the limited water [68]. Those results highly called attention to the parameterization of water stress using vegetation water indicators, instead of soil moisture only.

Vegetation indices are direct indicators of vegetation properties; thus are widely used in studies. In this research, we tried to use different vegetation indices to simulate the effect of water stress on the biogenic VOCs emission. It is found that the simulated results in southeastern China using the EDVI factor, especially daily EDVI factor, show better consistency with top-down retrieved emission than the simulation using soil moisture, NDVI or EVI. Soil moisture in southeastern China is always larger than the wilting point; thus affects the emission little. Optical vegetation indices, i.e., NDVI and EVI in this study, mainly reflect the properties of the top of the canopy, such as greenness. The microwave-based vegetation index, EDVI, presents the vegetation water content of the canopy crown due to the penetration of the microwaves. In additions, EDVI can be retrieved under clear sky and cloudy sky; thus reflecting the daily variation of vegetation water content.

It should be admitted that there are some limits to our study.

Firstly, there are a lack of proper observations that can be used as ground truth to directly evaluate the performance of simulated isoprene emission. Although there are some in situ measurement studies investigating the isoprene emission over China [69,70], the temporal ranges of those studies are relatively short. Until now, satellite observation is still the main way to constrain VOCs emissions in China. Therefore, there is an urgent need for more VOCs observation studies including in situ measurement and flight measurement in China.

Secondly, there is a lack of deep understanding of the physiological mechanisms to link isoprene emissions with EDVI. EDVI is a VWC indicator theoretically, but there are still no certain mathematical descriptions of EDVI to VWC and VWC to emissions also. The biogenic isoprene emission in water stress is linearly related to leaf water potential [58], but how to get the leaf water potential from the microwave-based vegetation index is unknown. Studies have shown that the relationships between water content and water potential are different among plant species [59,71]. However, there are already some studies that have connected leaf water potential and microwave-based vegetation index using a linear relationship [72]. So, in our study, using EDVI directly as the proxy of leaf water potential in a model is a reasonable trial of a way to estimate the water stress effects. To better understand the response of biogenic emission to water stress, studies related to EDVI and botanical process need to be carried out in future.

Thirdly, the temporal range of the study is limited. We conducted MEGAN simulations using different water stress factors only in 2008, while the performance of the EDVI factor in other years is unknown. It is shown that vegetation growth is affected by ENSO-induced precipitation change [73]. 2008 is La Niña year; thus the water stress may be affected and different to other years. So, whether the EDVI factor can present the water stress in other years, especially El Niño years, needs more investigation.

Despite the limitations, the comparison in this study mainly focuses on the temporal variations of the biogenic emissions in a large spatial scale, so satellite top-down retrieval emissions are the most proper data for the purpose. Satellite sensors can capture the temporal variations of atmospheric formaldehyde and provide the possibility to estimate the daily isoprene emissions in a large scale [40,74]. By comparing with the temporal variations of satellite top-down retrieval emissions, EDVI shows better controls on the isoprene emission rates than SM or VIs (NDVI and EVI) in southeastern China (Figure 7), which is an evidence of VWC effects on emissions.

The average top-down emission is lower than the modeled emission in this study, which is also found in some studies [38]. The EFs used in MEGAN are estimated using a closure measurement to measure the emission from branch or leaves, but the top-down retrieved emissions are related to the fluxes at the top of the canopy, thus the residue

within the canopy is one important reason [38]. So, it is noticed that the amount of isoprene residual within the canopy should be estimated in the coupled models.

5. Conclusions

Soil moisture cannot directly reflect the water stress on biogenic emissions because vegetation water content changes much slower than soil moisture. Aiming to study the vegetation water stress on biogenic emission, we applied soil moisture, EDVI, NDVI and EVI to the MEGAN model, and simulated isoprene emission in southeastern China during 2008. Compared with top-down retrieved emission, all of the simulations are found systematically larger, but spatially consistent, with correlation coefficients over 0.8. The simulated emission with EDVI is closest to top-down. From the temporal view, EDVI can significantly improve the simulation than soil moisture, NDVI and EVI. In those areas with dense vegetation, the simulations with EDVI applied are more consistent with top-down emissions with lower biases. Around Yunnan and the Yangtze River Delta, the temporal correlation coefficients increased by over 0.12 after using EDVI as the water stress factor, while others show little differences.

In conclusion, the simulated isoprene emission using the EDVI factor shows more consistent temporal variations compared with satellite top-down retrieval than using soil moisture or optical VIs in southeastern China, suggesting that the microwave-based vegetation index, i.e., EDVI, can be used in MEGAN to indicate the daily vegetation water stress on biogenic emission in southeastern China. More studies of EDVI and biogenic emissions are needed to improve our understanding of how the vegetation conditions influence the biogenic emissions.

Author Contributions: Conceptualization, Y.Z. and R.L.; methodology, Y.Z. and R.L.; software, Y.Z. and D.G.; validation, Y.Z., J.H. and Y.W.; formal analysis, Y.Z.; investigation, Y.Z.; resources, Y.Z., J.H. and Y.W.; data curation, J.H. and H.B.; writing—original draft preparation, Y.Z.; writing—review and editing, Y.Z., J.H., H.B., Y.F., Y.W. and R.L.; visualization, Y.Z.; supervision, Y.Z.; project administration, R.L.; funding acquisition, R.L. All authors have read and agreed to the published version of the manuscript.

Funding: This work was supported by National Key Research and Development Program of China (Grant No.2017YFC1501402), the National Natural Science Foundation of China NSFC (Grant No.41830104, 41661144007), and the Jiangsu Provincial 2011 Program (Collaborative Innovation Center of Climate Change).

Institutional Review Board Statement: Not applicable.

Informed Consent Statement: Not applicable.

Data Availability Statement: All of the research data and models are available online: EDVI data (<http://rse.ustc.edu.cn>, accessed on 31 December 2021); WRF model (<https://www2.mmm.ucar.edu/wrf/users/>, accessed on 31 December 2021); MEGAN model and the inputs (<https://bai.ess.uci.edu/megan/data-and-code>, accessed on 31 December 2021); OMI top-down retrieved isoprene emission (<https://emissions.aeronome.be/>, accessed on 31 December 2021); and MODIS Vegetation Indices (<https://lpdaac.usgs.gov/products/mod13c1v006/>, accessed on 31 December 2021).

Acknowledgments: The authors thank editors and reviewers for the critical and constructive suggestions.

Conflicts of Interest: The authors declare no conflict of interest.

Appendix A. Effects of Winter Snow on Vegetation Indices

Winter snow will cover the vegetation; thus affecting the satellite observed vegetation indices. We used MODIS MOD10C1 product to show snow cover, and analyzed the snow effects on microwave-based vegetation index (EDVI) and optical vegetation indices (NDVI and EVI) in the five regions selected. In regions 1 and 2, the winter snow is rare; thus the vegetation indices are affected little. While in region 3 and 4, winter snow largely affects the VIs. In the two regions, when the snow starts, EDVI increases, while NDVI and EVI

decrease to near 0. In region 5, although there are frequent snow events, the snow cover is relatively low; thus the effects on vegetation indices are also small.

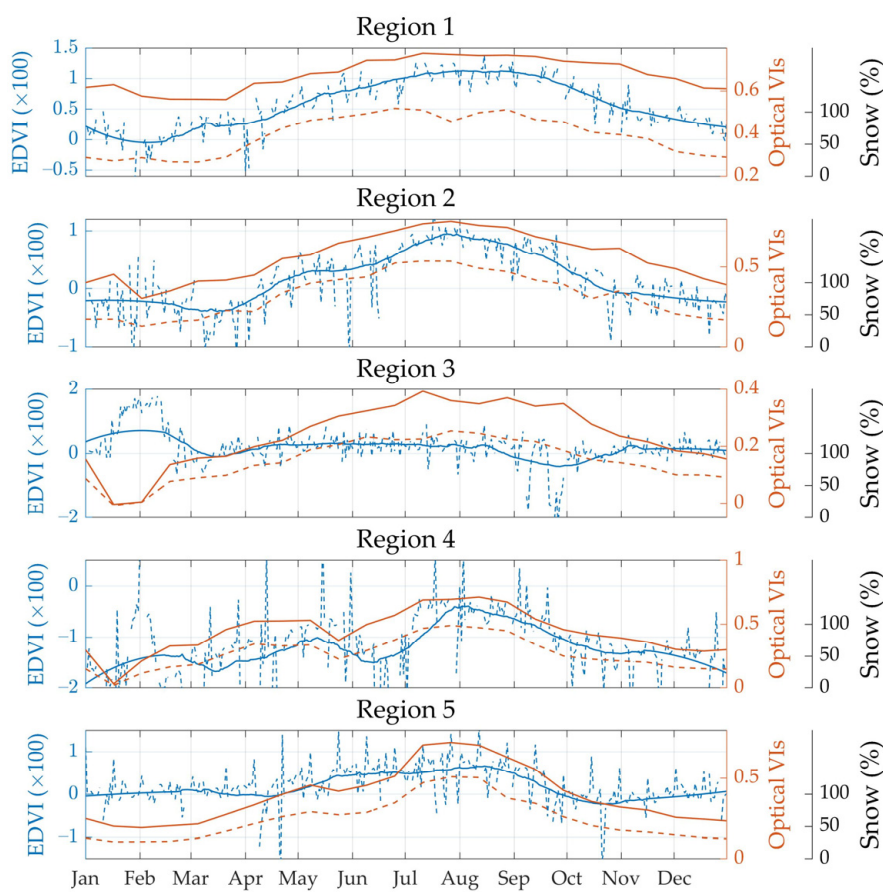


Figure A1. The time series of snow fraction (from MOD10C1, black bars), EDVI (blue line), NDVI (red line) and EVI (red dash line) in the selected five regions. The blue dash line denotes the daily EDVI, and the blue solid line denotes the smoothed EDVI.

References

- Churkina, G.; Kuik, F.; Bonn, B.; Lauer, A.; Grote, R.; Tomiak, K.; Butler, T.M. Effect of VOC Emissions from Vegetation on Air Quality in Berlin during a Heatwave. *Environ. Sci. Technol.* **2017**, *51*, 6120–6130. [[CrossRef](#)]
- Pang, X.; Mu, Y.; Zhang, Y.; Lee, X.; Yuan, J. Contribution of isoprene to formaldehyde and ozone formation based on its oxidation products measurement in Beijing, China. *Atmos. Environ.* **2009**, *43*, 2142–2147. [[CrossRef](#)]
- Sun, J.; Wu, F.; Hu, B.; Tang, G.; Zhang, J.; Wang, Y. VOC characteristics, emissions and contributions to SOA formation during hazy episodes. *Atmos. Environ.* **2016**, *141*, 560–570. [[CrossRef](#)]
- Pike, R.C.; Young, P.J. How plants can influence tropospheric chemistry: The role of isoprene emissions from the biosphere. *Weather* **2009**, *64*, 332–336. [[CrossRef](#)]
- Ying, Q.; Li, J.; Kota, S.H. Significant Contributions of Isoprene to Summertime Secondary Organic Aerosol in Eastern United States. *Environ. Sci. Technol.* **2015**, *49*, 7834–7842. [[CrossRef](#)] [[PubMed](#)]
- Nakashima, Y.; Tsurumaru, H.; Imamura, T.; Bejan, I.; Wenger, J.C.; Kajii, Y. Total OH reactivity measurements in laboratory studies of the photooxidation of isoprene. *Atmos. Environ.* **2012**, *62*, 243–247. [[CrossRef](#)]
- Sommariva, R.; Kramer, L.J.; Crilley, L.R.; Alam, M.S.; Bloss, W.J. An instrument for in situ measurement of total ozone reactivity. *Atmos. Meas. Tech.* **2020**, *13*, 1655–1670. [[CrossRef](#)]
- Matsumoto, J. Measurements of total ozone reactivity in a suburban forest in Japan. *Atmos. Environ.* **2021**, *246*, 117990. [[CrossRef](#)]
- Liu, Y.; Brito, J.; Dorris, M.R.; Rivera-Rios, J.C.; Seco, R.; Bates, K.H.; Artaxo, P.; Duvoisin, S.; Keutsch, F.N.; Kim, S.; et al. Isoprene photochemistry over the Amazon rainforest. *Proc. Natl. Acad. Sci. USA* **2016**, *113*, 6125–6130. [[CrossRef](#)]
- Silver, G.M.; Fall, R. Characterization of Aspen Isoprene Synthase, an Enzyme Responsible for Leaf Isoprene Emission to the Atmosphere. *J. Biol. Chem.* **1995**, *270*, 13010–13016. [[CrossRef](#)]
- Schnitzler, J.P.; Arenz, R.; Steinbrecher, R.; Lehning, A. Characterization of an Isoprene Synthase from Leaves of Quercus petraea (Mattuschka) Liebl. *Bot. Acta* **1996**, *109*, 216–221. [[CrossRef](#)]

12. Sharkey, T.D.; Singsaas, E.L. Why plants emit isoprene. *Nature* **1995**, *374*, 769. [[CrossRef](#)]
13. Singsaas, E.L.; Lerdau, M.; Winter, K.; Sharkey, T.D. Isoprene Increases Thermotolerance of Isoprene-Emitting Species. *Plant Physiol.* **1997**, *115*, 1413. [[CrossRef](#)]
14. Guenther, A.; Hewitt, C.N.; Erickson, D.; Fall, R.; Geron, C.; Graedel, T.; Harley, P.; Klinger, L.; Lerdau, M.; McKay, W.A.; et al. A global model of natural volatile organic compound emissions. *J. Geophys. Res. Atmos.* **1995**, *100*, 8873–8892. [[CrossRef](#)]
15. Kim, J.-C. Factors controlling natural VOC emissions in a southeastern US pine forest. *Atmos. Environ.* **2001**, *35*, 3279–3292. [[CrossRef](#)]
16. Peñuelas, J.; Llusia, J. The Complexity of Factors Driving Volatile Organic Compound Emissions by Plants. *Biol. Plant.* **2001**, *44*, 481–487. [[CrossRef](#)]
17. Owen, S.M.; Harley, P.; Guenther, A.; Hewitt, C.N. Light dependency of VOC emissions from selected Mediterranean plant species. *Atmos. Environ.* **2002**, *36*, 3147–3159. [[CrossRef](#)]
18. Kuhn, U.; Rottenberger, S.; Biesenthal, T.; Wolf, A.; Schebeske, G.; Ciccioli, P.; Brancaleoni, E.; Frattoni, M.; Tavares, T.M.; Kesselmeier, J. Seasonal differences in isoprene and light-dependent monoterpene emission by Amazonian tree species. *Glob. Change Biol.* **2004**, *10*, 663–682. [[CrossRef](#)]
19. Tarvainen, V.; Hakola, H.; Hellén, H.; Bäck, J.; Hari, P.; Kulmala, M. Temperature and light dependence of the VOC emissions of Scots pine. *Atmos. Chem. Phys.* **2005**, *5*, 989–998. [[CrossRef](#)]
20. Sharkey, T.D.; Loreto, F. Water stress, temperature, and light effects on the capacity for isoprene emission and photosynthesis of kudzu leaves. *Oecologia* **1993**, *95*, 328–333. [[CrossRef](#)]
21. Peñuelas, J.; Filella, I.; Seco, R.; Llusia, J. Increase in isoprene and monoterpene emissions after re-watering of droughted *Quercus ilex* seedlings. *Biol. Plant.* **2009**, *53*, 351–354. [[CrossRef](#)]
22. Guidolotti, G.; Calfapietra, C.; Loreto, F. The relationship between isoprene emission, CO₂ assimilation and water use efficiency across a range of poplar genotypes. *Physiol. Plant.* **2011**, *142*, 297–304. [[CrossRef](#)] [[PubMed](#)]
23. Brilli, F.; Tsonev, T.; Mahmood, T.; Velikova, V.; Loreto, F.; Centritto, M. Ultradian variation of isoprene emission, photosynthesis, mesophyll conductance, and optimum temperature sensitivity for isoprene emission in water-stressed *Eucalyptus citriodora* saplings. *J. Exp. Bot.* **2013**, *64*, 519–528. [[CrossRef](#)] [[PubMed](#)]
24. Guenther, A.; Zimmerman, P.; Wildermuth, M. Natural volatile organic compound emission rate estimates for U.S. woodland landscapes. *Atmos. Environ.* **1994**, *28*, 1197–1210. [[CrossRef](#)]
25. Kesselmeier, J.; Kuhn, U.; Wolf, A.; Andreae, M.O.; Ciccioli, P.; Brancaleoni, E.; Frattoni, M.; Guenther, A.; Greenberg, J.; De Castro Vasconcellos, P.; et al. Atmospheric volatile organic compounds (VOC) at a remote tropical forest site in central Amazonia. *Atmos. Environ.* **2000**, *34*, 4063–4072. [[CrossRef](#)]
26. Sharkey, T.D.; Wiberley, A.E.; Donohue, A.R. Isoprene Emission from Plants: Why and How. *Ann. Bot.* **2008**, *101*, 5–18. [[CrossRef](#)]
27. Alves, E.G.; Harley, P.; de Carvalho Gonçalves, J.F.; da Silva Moura, C.E.; Jardine, K. Effects of light and temperature on isoprene emission at different leaf developmental stages of eschweilera coriacea in central Amazon. *Acta Amaz.* **2014**, *44*, 9–18. [[CrossRef](#)]
28. Guenther, A.; Karl, T.; Harley, P.; Wiedinmyer, C.; Palmer, P.I.; Geron, C. Estimates of global terrestrial isoprene emissions using MEGAN (Model of Emissions of Gases and Aerosols from Nature). *Atmos. Chem. Phys.* **2006**, *6*, 3181–3210. [[CrossRef](#)]
29. Lathière, J.; Hauglustaine, D.A.; Friend, A.D.; De Noblet-Ducoudré, N.; Viovy, N.; Folberth, G.A. Impact of climate variability and land use changes on global biogenic volatile organic compound emissions. *Atmos. Chem. Phys.* **2006**, *6*, 2129–2146. [[CrossRef](#)]
30. Müller, J.F.; Stavrakou, T.; Wallens, S.; De Smedt, I.; Van Roozendael, M.; Potosnak, M.J.; Rinne, J.; Munger, B.; Goldstein, A.; Guenther, A.B. Global isoprene emissions estimated using MEGAN, ECMWF analyses and a detailed canopy environment model. *Atmos. Chem. Phys.* **2008**, *8*, 1329–1341. [[CrossRef](#)]
31. Levis, S.; Wiedinmyer, C.; Bonan, G.B.; Guenther, A. Simulating biogenic volatile organic compound emissions in the Community Climate System Model. *J. Geophys. Res. Atmos.* **2003**, *108*, 4659. [[CrossRef](#)]
32. Abbot Dorian, S.; Palmer Paul, I.; Martin Randall, V.; Chance Kelly, V.; Jacob Daniel, J.; Guenther, A. Seasonal and interannual variability of North American isoprene emissions as determined by formaldehyde column measurements from space. *Geophys. Res. Lett.* **2003**, *30*, 111. [[CrossRef](#)]
33. Millet, D.B.; Jacob, D.J.; Turquety, S.; Hudman, R.C.; Wu, S.; Fried, A.; Walega, J.; Heikes, B.G.; Blake, D.R.; Singh, H.B.; et al. Formaldehyde distribution over North America: Implications for satellite retrievals of formaldehyde columns and isoprene emission. *J. Geophys. Res. Atmos.* **2006**, *111*, D24S02. [[CrossRef](#)]
34. Palmer, P.I.; Jacob, D.J.; Fiore, A.M.; Martin, R.V.; Chance, K.; Kurosu, T.P. Mapping isoprene emissions over North America using formaldehyde column observations from space. *J. Geophys. Res. Atmos.* **2003**, *108*, 4180. [[CrossRef](#)]
35. Palmer, P.I.; Abbot, D.S.; Fu, T.-M.; Jacob, D.J.; Chance, K.; Kurosu, T.P.; Guenther, A.; Wiedinmyer, C.; Stanton, J.C.; Pilling, M.J.; et al. Quantifying the seasonal and interannual variability of North American isoprene emissions using satellite observations of the formaldehyde column. *J. Geophys. Res. Atmos.* **2006**, *111*, D12315. [[CrossRef](#)]
36. Shim, C.; Wang, Y.; Choi, Y.; Palmer, P.I.; Abbot, D.S.; Chance, K. Constraining global isoprene emissions with Global Ozone Monitoring Experiment (GOME) formaldehyde column measurements. *J. Geophys. Res. Atmos.* **2005**, *110*, 0148–0227. [[CrossRef](#)]
37. Barkley, M.P.; Palmer, P.I.; Kuhn, U.; Kesselmeier, J.; Chance, K.; Kurosu, T.P.; Martin, R.V.; Helmig, D.; Guenther, A. Net ecosystem fluxes of isoprene over tropical South America inferred from Global Ozone Monitoring Experiment (GOME) observations of HCHO columns. *J. Geophys. Res. Atmos.* **2008**, *113*, D20304. [[CrossRef](#)]

38. Millet, D.B.; Jacob, D.J.; Boersma, K.F.; Fu, T.-M.; Kurosu, T.P.; Chance, K.; Heald, C.L.; Guenther, A. Spatial distribution of isoprene emissions from North America derived from formaldehyde column measurements by the OMI satellite sensor. *J. Geophys. Res. Atmos.* **2008**, *113*, D02307. [\[CrossRef\]](#)
39. Marais, E.A.; Jacob, D.J.; Guenther, A.; Chance, K.; Kurosu, T.P.; Murphy, J.G.; Reeves, C.E.; Pye, H.O.T. Improved model of isoprene emissions in Africa using Ozone Monitoring Instrument (OMI) satellite observations of formaldehyde: Implications for oxidants and particulate matter. *Atmos. Chem. Phys.* **2014**, *14*, 7693–7703. [\[CrossRef\]](#)
40. De Smedt, I.; Stavrakou, T.; Hendrick, F.; Danckaert, T.; Vlemmix, T.; Pinardi, G.; Theys, N.; Lerot, C.; Gielen, C.; Vigouroux, C.; et al. Diurnal, seasonal and long-term variations of global formaldehyde columns inferred from combined OMI and GOME-2 observations. *Atmos. Chem. Phys.* **2015**, *15*, 12519–12545. [\[CrossRef\]](#)
41. Stavrakou, T.; Müller, J.F.; Bauwens, M.; De Smedt, I.; Van Roozendael, M.; De Mazière, M.; Vigouroux, C.; Hendrick, F.; George, M.; Clerbaux, C.; et al. How consistent are top-down hydrocarbon emissions based on formaldehyde observations from GOME-2 and OMI? *Atmos. Chem. Phys.* **2015**, *15*, 11861–11884. [\[CrossRef\]](#)
42. Monson, R.K.; Fall, R. Isoprene Emission from Aspen Leaves. *Plant Physiol.* **1989**, *90*, 267. [\[CrossRef\]](#) [\[PubMed\]](#)
43. de Souza, V.F.; Niinemets, Ü.; Rasulov, B.; Vickers, C.E.; Duvoisin Júnior, S.; Araújo, W.L.; de Carvalho Gonçalves, J.F. Alternative Carbon Sources for Isoprene Emission. *Trends Plant Sci.* **2018**, *23*, 1081–1101. [\[CrossRef\]](#) [\[PubMed\]](#)
44. Pegoraro, E.; Rey, A.; Bobich, E.G.; Barron-Gafford, G.; Grieve, K.A.; Malhi, Y.; Murthy, R. Effect of elevated CO₂ concentration and vapour pressure deficit on isoprene emission from leaves of *Populus deltoides* during drought. *Funct. Plant Biol.* **2004**, *31*, 1137–1147. [\[CrossRef\]](#)
45. Guenther, A.B.; Jiang, X.; Heald, C.L.; Sakulyanontvittaya, T.; Duhl, T.; Emmons, L.K.; Wang, X. The Model of Emissions of Gases and Aerosols from Nature version 2.1 (MEGAN2.1): An extended and updated framework for modeling biogenic emissions. *Geosci. Model Dev.* **2012**, *5*, 1471–1492. [\[CrossRef\]](#)
46. Llusià, J.; Peñuelas, J. Changes in terpene content and emission in potted Mediterranean woody plants under severe drought. *Can. J. Bot.* **1998**, *76*, 1366–1373. [\[CrossRef\]](#)
47. Geron, C.; Owen, S.; Guenther, A.; Greenberg, J.; Rasmussen, R.; Hui Bai, J.; Li, Q.-J.; Baker, B. Volatile organic compounds from vegetation in southern Yunnan Province, China: Emission rates and some potential regional implications. *Atmos. Environ.* **2006**, *40*, 1759–1773. [\[CrossRef\]](#)
48. Sindelarova, K.; Granier, C.; Bouarar, I.; Guenther, A.; Tilmes, S.; Stavrakou, T.; Müller, J.F.; Kuhn, U.; Stefani, P.; Knorr, W. Global data set of biogenic VOC emissions calculated by the MEGAN model over the last 30 years. *Atmos. Chem. Phys.* **2014**, *14*, 9317–9341. [\[CrossRef\]](#)
49. Bauwens, M.; Stavrakou, T.; Müller, J.F.; De Smedt, I.; Van Roozendael, M.; van der Werf, G.R.; Wiedinmyer, C.; Kaiser, J.W.; Sindelarova, K.; Guenther, A. Nine years of global hydrocarbon emissions based on source inversion of OMI formaldehyde observations. *Atmos. Chem. Phys.* **2016**, *16*, 10133–10158. [\[CrossRef\]](#)
50. Jiang, X.; Guenther, A.; Potosnak, M.; Geron, C.; Seco, R.; Karl, T.; Kim, S.; Gu, L.; Pallardy, S. Isoprene emission response to drought and the impact on global atmospheric chemistry. *Atmos. Environ.* **2018**, *183*, 69–83. [\[CrossRef\]](#)
51. Tingey, D.T.; Evans, R.; Gumpertz, M. Effects of environmental conditions on isoprene emission from live oak. *Planta* **1981**, *152*, 565–570. [\[CrossRef\]](#) [\[PubMed\]](#)
52. Brilli, F.; Barta, C.; Fortunati, A.; Lerdau, M.; Loreto, F.; Centritto, M. Response of isoprene emission and carbon metabolism to drought in white poplar (*Populus alba*) saplings. *New Phytol.* **2007**, *175*, 244–254. [\[CrossRef\]](#) [\[PubMed\]](#)
53. Rodríguez-Calcerrada, J.; Buatois, B.; Chiche, E.; Shahin, O.; Staudt, M. Leaf isoprene emission declines in *Quercus pubescens* seedlings experiencing drought—Any implication of soluble sugars and mitochondrial respiration? *Environ. Exp. Bot.* **2013**, *85*, 36–42. [\[CrossRef\]](#)
54. Henrot, A.J.; Stanelle, T.; Schröder, S.; Siegenthaler, C.; Taraborrelli, D.; Schultz, M.G. Implementation of the MEGAN (v2.1) biogenic emission model in the ECHAM6-HAMMOZ chemistry climate model. *Geosci. Model Dev.* **2017**, *10*, 903–926. [\[CrossRef\]](#)
55. Otu-Larbi, F.; Bolas, C.G.; Ferracci, V.; Staniaszek, Z.; Jones, R.L.; Malhi, Y.; Harris, N.R.P.; Wild, O.; Ashworth, K. Modelling the effect of the 2018 summer heatwave and drought on isoprene emissions in a UK woodland. *Glob. Change Biol.* **2019**, *26*, 2320–2335. [\[CrossRef\]](#)
56. Plaza, J.; Núñez, L.; Pujadas, M.; Pérez-Pastor, R.; Bermejo, V.; García-Alonso, S.; Elvira, S. Field monoterpane emission of Mediterranean oak (*Quercus ilex*) in the central Iberian Peninsula measured by enclosure and micrometeorological techniques: Observation of drought stress effect. *J. Geophys. Res. Atmos.* **2005**, *110*, D03303. [\[CrossRef\]](#)
57. Pegoraro, E.; Rey, A.N.A.; Abrell, L.; Van Haren, J.; Lin, G. Drought effect on isoprene production and consumption in Biosphere 2 tropical rainforest. *Glob. Change Biol.* **2006**, *12*, 456–469. [\[CrossRef\]](#)
58. Pegoraro, E.; Rey, A.; Greenberg, J.; Harley, P.; Grace, J.; Malhi, Y.; Guenther, A. Effect of drought on isoprene emission rates from leaves of *Quercus virginiana* Mill. *Atmos. Environ.* **2004**, *38*, 6149–6156. [\[CrossRef\]](#)
59. Kalapos, T. Leaf water potential-leaf water deficit relationship for ten species of a semiarid grassland community. *Plant Soil* **1994**, *160*, 105–112. [\[CrossRef\]](#)
60. Min, Q.; Lin, B. Determination of spring onset and growing season leaf development using satellite measurements. *Remote Sens. Environ.* **2006**, *104*, 96–102. [\[CrossRef\]](#)
61. Li, R.; Min, Q.; Lin, B. Estimation of evapotranspiration in a mid-latitude forest using the Microwave Emissivity Difference Vegetation Index (EDVI). *Remote Sens. Environ.* **2009**, *113*, 2011–2018. [\[CrossRef\]](#)

62. Zhang, Y.; Li, R.; Min, Q.; Bo, H.; Fu, Y.; Wang, Y.; Gao, Z. The Controlling Factors of Atmospheric Formaldehyde (HCHO) in Amazon as Seen From Satellite. *Earth Space Sci.* **2019**, *6*, 959–971. [[CrossRef](#)]
63. Dy, C.Y.; Fung, J.C.H. Updated global soil map for the Weather Research and Forecasting model and soil moisture initialization for the Noah land surface model. *J. Geophys. Res. Atmos.* **2016**, *121*, 8777–8800. [[CrossRef](#)]
64. Du, Q.; Zhao, C.; Zhang, M.; Dong, X.; Chen, Y.; Liu, Z.; Hu, Z.; Zhang, Q.; Li, Y.; Yuan, R.; et al. Modeling diurnal variation of surface PM2.5 concentrations over East China with WRF-Chem: Impacts from boundary-layer mixing and anthropogenic emission. *Atmos. Chem. Phys.* **2020**, *20*, 2839–2863. [[CrossRef](#)]
65. Hu, J.; Fu, Y.; Zhang, P.; Min, Q.; Gao, Z.; Wu, S.; Li, R. Satellite Retrieval of Microwave Land Surface Emissivity under Clear and Cloudy Skies in China Using Observations from AMSR-E and MODIS. *Remote Sens.* **2021**, *13*, 3980. [[CrossRef](#)]
66. Min, Q.; Lin, B. Remote sensing of evapotranspiration and carbon uptake at Harvard Forest. *Remote Sens. Environ.* **2006**, *100*, 379–387. [[CrossRef](#)]
67. Li, R.; Wang, Y.; Hu, J.; Wang, Y.; Min, Q.; Bergeron, Y.; Valeria, O.; Gao, Z.; Liu, J.; Fu, Y. Spatiotemporal Variations of Satellite Microwave Emissivity Difference Vegetation Index in China Under Clear and Cloudy Skies. *Earth Space Sci.* **2020**, *7*, e2020EA001145. [[CrossRef](#)]
68. Zheng, Y.; Unger, N.; Tadić, J.M.; Seco, R.; Guenther, A.B.; Barkley, M.P.; Potosnak, M.J.; Murray, L.T.; Michalak, A.M.; Qiu, X.; et al. Drought impacts on photosynthesis, isoprene emission and atmospheric formaldehyde in a mid-latitude forest. *Atmos. Environ.* **2017**, *167*, 190–201. [[CrossRef](#)]
69. Bai, J.; Baker, B.; Liang, B.; Greenberg, J.; Guenther, A. Isoprene and monoterpene emissions from an Inner Mongolia grassland. *Atmos. Environ.* **2006**, *40*, 5753–5758. [[CrossRef](#)]
70. Klinger, L.F.; Li, Q.J.; Guenther, A.B.; Greenberg, J.P.; Baker, B.; Bai, J.H. Assessment of volatile organic compound emissions from ecosystems of China. *J. Geophys. Res. Atmos.* **2002**, *107*, ACH 16-11–ACH 16-21. [[CrossRef](#)]
71. Wijewardana, C.; Alsajri, F.A.; Irby, J.T.; Krutz, L.J.; Golden, B.; Henry, W.B.; Gao, W.; Reddy, K.R. Physiological assessment of water deficit in soybean using midday leaf water potential and spectral features. *J. Plant Interact.* **2019**, *14*, 533–543. [[CrossRef](#)]
72. Zhang, Y.; Zhou, S.; Gentine, P.; Xiao, X. Can vegetation optical depth reflect changes in leaf water potential during soil moisture dry-down events? *Remote Sens. Environ.* **2019**, *234*, 111451. [[CrossRef](#)]
73. Shuai, J.; Zhang, Z.; Tao, F.; Shi, P. How ENSO affects maize yields in China: Understanding the impact mechanisms using a process-based crop model. *Int. J. Climatol.* **2016**, *36*, 424–438. [[CrossRef](#)]
74. Barkley, M.P.; Smedt, I.D.; Van Roozendael, M.; Kurosu, T.P.; Chance, K.; Arneth, A.; Hagberg, D.; Guenther, A.; Paulot, F.; Marais, E.; et al. Top-down isoprene emissions over tropical South America inferred from SCIAMACHY and OMI formaldehyde columns. *J. Geophys. Res. Atmos.* **2013**, *118*, 6849–6868. [[CrossRef](#)]